2,3,5,6-Tetrasilyl- and 2,3,5,6-Tetragermyl-1,4-benzoquinones: X-ray Crystallographic Analysis, Cyclic Voltammetry, and DFT Calculations

Shinobu Tsutsui,*,† Kenkichi Sakamoto,*,†,‡ Hiroto Yoshida,§ and Atsutaka Kunai§

Photodynamics Research Center, The Institute of Physical and Chemical Research (RIKEN), 519-1399 Aoba, Aramaki, Aoba-ku, Sendai 980-0845, Japan, Department of Chemistry, Graduate School of Science, Tohoku University, Aoba-ku, Sendai 980-8578, Japan, and Department of Applied Chemistry, Graduate School of Engineering, Hiroshima University, Higashi-Hiroshima 739-8527, Japan

Received November 26, 2003

By X-ray crystallographic analysis, it was proved that 2,3,5,6-tetrakis(trimethylgermyl)-1,4-benzoquinone, 2,3,5,6-tetrakis(dimethylvinylsilyl)-1,4-benzoquinone, and 2,3,5-tris(trimethylsilyl)-1,4-benzoquinone took a chair conformation, while 4,4,6,6,10,10,12,12-octamethyl-4,6,10,12-tetrasilatricyclo[7.3.0.0^{3,7}]dodeca-1(9),3(7)-diene-2,8-dione had a planar structure. Cyclic voltammograms of 2,5-bis(trimethylsilyl)-1,4-benzoquinone (**5a**) and 1,4-benzoquinone (**1f**) showed two sets of reversible redox peaks. On the other hand, the voltammogram of 2,3,5,6-tetrakis(trimethylsilyl)-1,4-benzoquinone (**1a**) showed that the first reduction step was reversible and the second step was irreversible. The first reduction potential of **1a** ($E_{1/2}^{I}$ = −1.12 V vs Ag/Ag$^+$) was higher by more than 0.2 V compared to those of **5a** ($E_{1/2}^{I}$ = −0.88 V) and **1f** ($E_{1/2}^{I}$ = −0.81 V). DFT calculations for trimethylsilyl-substituted 1,4-benzoquinones revealed that the LUMOs shifted to higher energies, whereas the calculated vibrational frequencies shifted to lower frequencies as the number of silyl groups increased. These results demonstrated that the trimethylsilyl group acted as an electron-donating group to the 1,4-benzoquinone unit.

Introduction

1,4-Benzoquinone (quinone) is one of the most important and fundamental π-electron systems because of its high electron affinity and photoreactivity.[1] Although there have been a large number of reports on 1,4-benzoquinone derivatives, very few studies on the silyl- and germyl-1,4-benzoquinones have been conducted.[2−9] Thus, the chemistry of silyl-substituted 1,4-benzoquinones is of great interest from the viewpoints of the well-known electronic effects and steric hindrance of silyl groups toward π-electron systems.[10] Recently, we have reported the preparation, structures, and novel photoreactivities of 2,3,5,6-tetrasilyl-1,4-benzoquinone derivatives.[8,9] Namely, X-ray crystallographic analysis revealed that 2,3,5,6-tetrakis(trimethylsilyl)-1,4-benzoquinone (**1a**, Chart 1) takes the chair conformation, and the deformed quinone ring allows a $\sigma(C_{quinone}-Si)-\pi^*$ electronic transition at 403 nm in **1a**. Thus, photolysis of **1a** results in isomerization, creating a ketene derivative, 4-carbonyl-2,3,5,5-tetrakis(trimethylsilyl)-2-cyclopenten-1-one (**2**). In contrast to **1a**, 2,3,5,6-tetrakis(dimethylsilyl)-1,4-benzoquinone (**1b**) has an almost planar quinone ring and photolysis does not induce isomerization. We also succeeded in the preparation of a number of derivatives including 2,3,5,6-tetrakis(trimethylgermyl)-1,4-benzoquinone (**1c**), which was the first report of a 2,3,5,6-tetragermyl-1,4,-benzoquinone derivative, 2,3,5,6-tetrakis(dimethylvinylsilyl)-1,4-benzoquinone (**1d**), 4,4,6,6,10,10,12,12-octamethyl-4,6,10,-

* Corresponding authors. E-mail: stsutsui@riken.jp; sakamoto@si.chem.tohoku.ac.jp.
† RIKEN.
‡ Tohoku University.
§ Hiroshima University.

(1) For reviews on quinones. See: (a) Thomson, R. H. In *The Chemistry of the Quinonoid Compounds*; Patai, S., Ed.; John Wiley & Sons: Bristol, 1974. (b) Naruta, Y.; Maruyama, K. In *The Chemistry of the Quinonoid Compounds*; Patai, S., Rappoport, Z., Eds.; John Wiley & Sons: New York, 1988; Vol. 2.
(2) (a) Cooper, G. D.; Williams, B.; Lape, C. P. *J. Org. Chem.* **1961**, *26*, 4171. (b) Hashimoto, H. *Yakugaku Zasshi* **1967**, *87*, 535.
(3) (a) Bock, H.; Alt, H. *Angew. Chem., Int. Ed. Engl.* **1967**, *6*, 941. (b) Bock, H.; Nick, S.; Nather, C.; Ruppert, K. *Z. Naturforsch., B* **1995**, *50*, 595.
(4) (a) Vasileiskaya, N. S.; Gorbunova, L. V.; Mamysheva, O. N.; Bortnikov, G. N. *Izv. Akad. Nauk. SSSR, Ser. Khim.* **1972**, 2755. (b) Foland, L. D.; Karlsson, J. O.; Perri, S. T.; Schwabe, R.; Xu, S. L.; Patil, S.; Moore H. W. *J. Am. Chem. Soc.* **1989**, *111*, 975. (c) Oleinik, É. P.; Mamysheva, O. N.; Gorbunova, L. V. *Dokl. Akad. Nauk SSSR* **1986**, *289*, 1137.
(5) (a) Sakamoto, K.; Sakurai, H. *J. Am. Chem. Soc.* **1991**, *113*, 1466. (b) Sakurai, H., Abe, J.; Sakamoto, K. *J. Photochem. Photobiol., A* **1992**, *65*, 111.
(6) Tsutsui, S.; Sakamoto, K.; Ebata, K.; Kabuto, C.; Sakurai, H. *Bull. Chem. Soc. Jpn.* **2002**, *75*, 2661.
(7) Tsutsui, S.; Sakamoto, K. *Chem. Commun.* **2003**, 2322.
(8) Sakamoto, K.; Tsutsui, S.; Ebata, K.; Kabuto, C.; Sakurai, H. *Chem. Lett.* **2000**, 226.
(9) Tsutsui, S.; Sakamoto, K.; Ebata, K.; Kabuto, C.; Sakurai, H. *Bull. Chem. Soc. Jpn.* **2002**, *75*, 2571.
(10) Reviews for silyl-substituted π-electron systems. (a) Sakurai, H. *Nippon Kagaku Kaishi* **1990**, 439. (b) Sakurai, H. *Pure Appl. Chem.* **1996**, *68*, 327.

10.1021/om034325a CCC: $27.50
Publication on Web 03/02/2004

Chart 1

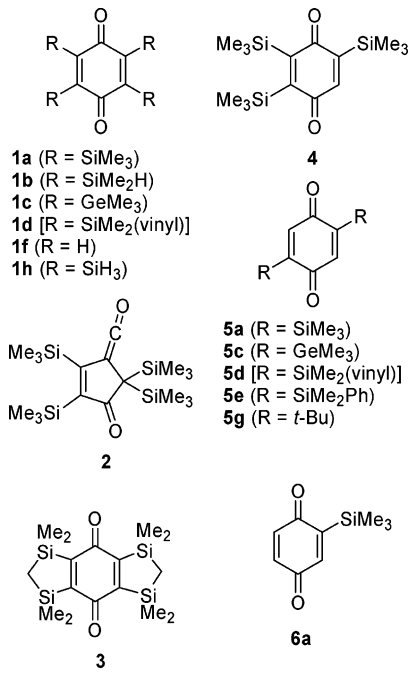

12-tetrasilatricyclo[7.3.0.0^{3,7}]dodeca-1(9),3(7)-diene-2,8-dione (**3**), and 2,3,5-tris(trimethylsilyl)-1,4-benzoquinone (**4**). The electronic absorption spectra of **1c**, **1d**, and **4** show the σ[$C_{quinone}$−Si (or Ge)]−π* bands, whereas **3** did not show the corresponding transition band in the UV−vis spectrum. The findings suggest that **1c**, **1d**, and **4** are in the chair conformation, while **3** has a planar structure. The solid structures of **1c**, **1d**, **3**, and **4**, however, have yet to be successfully analyzed. Herein, we report the X-ray crystallographic analysis of **1c**, **1d**, **3**, **4**, and the related germyl- and silyl-substituted 1,4-benzoquinones: 2,5-bis(trimethylgermyl)-1,4-benzoquinone (**5c**), 2,5-bis(dimethylvinylsilyl)-1,4-benzoquinone (**5d**), and 2,5-bis(dimethylphenylsilyl)-1,4-benzoquinone (**5e**).

1,4-Benzoquinone derivatives usually undergo two-step, one-electron reductions in aprotic solvents to form radical anions and dianions. In 1967, Bock et al. reported the half-reduction potentials of 2,5-bis(trimethylsilyl)-1,4-benzoquinone (**5a**), 2,5-di-*tert*-butyl-1,4-benzoquinone (**5g**), and 1,4-benzoquinone (**1f**) in acetonitrile with tetra-*n*-butylammonium iodide as the supporting electrolyte against a constant mercury anode.[3a] Herein, we also report the electrochemical properties of **1a**, compared with those of **1f**, **5a**, **5g**, and 2-(trimethylsilyl)-1,4-benzoquinone (**6a**). In an effort to elucidate the energies and electronic structures of **1a**, **5a**, **6a**, **1f**, and **5g**, density functional theory (DFT) calculations were performed.

Results and Discussion

X-ray Crystallographic Analysis. Silyl- and germyl-1,4-benzoquinones **1c**, **1d**, **3**, **4**, and **5c**−**e** (Chart 1) were prepared according to the procedures previously reported.[9] Recrystallization using hexane gave single crystals of these compounds, suitable for X-ray structural analysis. Figures 1−7 show perspective views of the molecular structures of **1c**, **1d**, **3**, **4**, and **5c**−**e**, respectively. Selected bond lengths and angles for **1a**−**d** and **3** and those for **5a** and **5c**−**e** are listed in Tables 1 and 2, respectively. Crystal data for **1c**, **1d**, **3**, **4**, and **5c**−**e** are summarized in the Experimental Section.

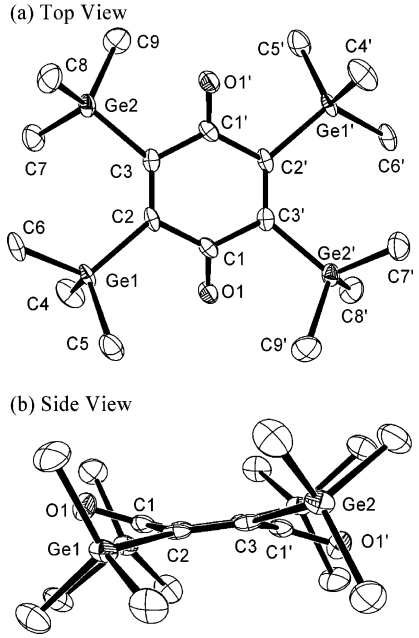

Figure 1. Top (a) and side (b) ORTEP views of **1c** showing the atom-numbering scheme. Dashes indicate atoms related by symmetry. Thermal ellipsoids are drawn at the 50% probability level. Hydrogen atoms are omitted for clarity. Selected bond lengths (Å): C(1)−O(1) = 1.216(6), C(1)−C(2) = 1.494(7), C(1)−C(3′) = 1.510(7), C(2)−C(3) = 1.365(7), C(2)−Ge(1) = 1.985(5), C(3)−Ge(2) = 1.980(5), C(methyl)−Ge(1) = 1.941(6)−1.965(7). Selected bond angles (deg): O(1)−C(1)−C(2) = 118.9(5), O(1)−C(1)−C(3′) = 118.0(5), C(2)−C(1)−C(3′) = 122.7(5), C(3)−C(2)−C(1) = 118.0(5), C(3)−C(2)−Ge(1) = 130.2(4), C(1)−C(2)−Ge(1) = 111.7(4), C(2)−C(3)−C(1′) = 116.4(5), C(2)−C(3)−Ge(2) = 130.7(4), C(1′)−C(3)−Ge(2) = 112.9(4), C(methyl)−Ge−C(methyl) = 104.4(3)−113.1(3), C(quinone)−Ge−C(methyl) = 107.6(2)−111.4(2).

Figure 1 shows that the quinone ring of **1c** was significantly distorted into the chair conformation by the steric repulsion between the pairs of vicinal trimethylgermyl groups. The torsion angles for Ge1−C2═C3−Ge2 and C1−C2═C3−C1′ were 14.0(8)° and 18.8(7)°, respectively. The sum of the angles around C2 (359.9°) and C3 (360.0°) indicates that the sp^2 carbon atoms remained in near-planar geometries. As shown in Table 2, the bond length of **1c** for C2═C3 (1.365 Å) was slightly longer than the length of the corresponding carbon−carbon bond in **1a** (1.354 Å). The angle between the planes defined by C1−C2−C3′ and C2−C3−C2′−C3′ of **1c** was 17.6(5)°, which was almost the same as the corresponding angle in **1a** (19.1°).

Figure 2 indicates that the quinone ring of **1d** was in the chair conformation in order to relieve the steric repulsion between the pairs of vicinal dimethylvinylsilyl groups. The torsion angles for Si1−C2═C3−Si2 and C1−C2═C3−C1′ were 22.1(3)° and 18.8(3)°, respectively. The vinyl group on the Si2 atom was directed toward the C1′═O1′ group. However, the vinyl group on the Si1 atom was not directed toward the C1═O1, but the vicinal dimethylvinylsilyl group. As shown in Table 2, the bond length of **1d** for C2═C3 (1.360 Å) was in good agreement with the length of the corresponding carbon−carbon bond in **1c** (1.361 Å). The angle between

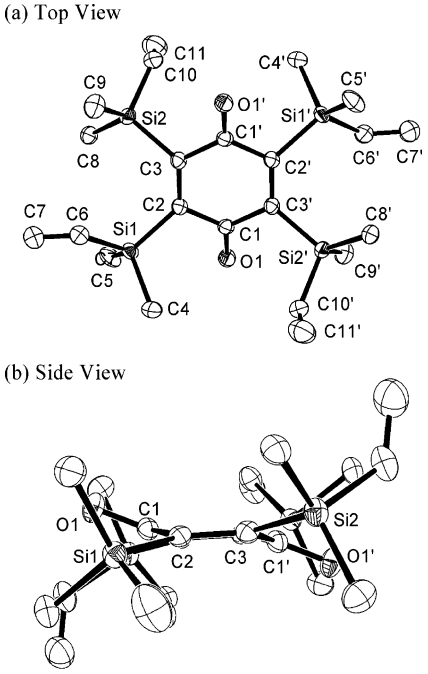

Figure 2. Top (a) and side (b) ORTEP views of **1d** showing the atom-numbering scheme. Dashes indicate atoms related by symmetry. Thermal ellipsoids are drawn at the 50% probability level. Hydrogen atoms are omitted for clarity. Selected bond lengths (Å): C(1)−O(1) = 1.227(2), C(1)−C(2) = 1.495(3), C(1)−C(3)′ = 1.499(2), C(2)−C(3) = 1.360(3), C(2)−Si(1) = 1.9112(18), C(3)−Si(2) = 1.9100(19), C(Methyl)−Si = 1.860(2)−1.864(2), C(6)−C(7) = 1.311(3), C(6)−Si(1) = 1.871(2), C(10)−C(11) = 1.274(3), C(10)−Si(2) = 1.854(2). Selected bond angles (deg): O(1)−C(1)−C(2) = 118.01(16), O(1)−C(1)−C(3)′ = 117.89(17), C(2)−C(1)−C(3)′ = 123.65(16), C(3)−C(2)−C(1) = 116.74(15), C(3)−C(2)−Si(1) = 130.09(14), C(1)−C(2)−Si(1) = 113.14(12), C(2)−C(3)−C(1)′ = 116.62(16), C(2)−C(3)−Si(2) = 130.34(14), C(1)′−C(3)−Si(2) = 113.03(13), C(5)−Si(1)−C(4) = 108.92(10), C(methyl)−Si(1)−C(vinyl) = 105.03(10)−111.19(11), C(methyl)−Si−C(quinone) = 107.99(9)−114.24(9), C(6)−Si(1)−C(2) = 109.02(9), C(8)−Si(2)−C(9) = 112.87(10), C(10)−Si(2)−C(3) = 107.27(9).

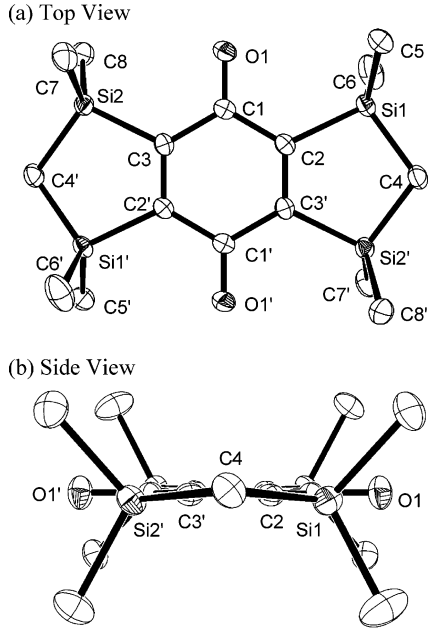

Figure 3. Top (a) and side (b) ORTEP views of **3** showing the atom-numbering scheme. Dashes indicate atoms related by symmetry. Thermal ellipsoids are drawn at the 50% probability level. Hydrogen atoms are omitted for clarity. Selected bond lengths (Å): C(1)−O(1) =1.235(2), C(1)−C(2) = 1.489(3), C(1)−C(3) = 1.500(3), C(2)−C(3)′ = 1.362(3), C(2)−Si(1) = 1.908(2), C(3)−Si(2) = 1.902(2), C(4)−Si(2)′ = 1.880(2), C(4)−Si(1) = 1.880(2), C(methyl)−Si = 1.863(2)−1.874(2). Selected bond angles (deg): O(1)−C(1)−C(2) = 120.44(19), O(1)−C(1)−C(3) = 120.28(19), C(2)−C(1)−C(3) = 119.28(18), C(3)′−C(2)−C(1) = 120.16-(19), C(3)′−C(2)−Si(1) = 116.12(16), C(1)−C(2)−Si(1) = 123.71(15), C(2)′−C(3)−C(1) = 120.55(19), C(2)′−C(3)−Si-(2) = 116.18(16), C(1)−C(3)−Si(2) = 123.23(15), Si(2)′-C(4)−Si(1) = 107.93(10), C(4)−Si(1)−C(2) = 99.27(9), C(4)′−Si(2)−C(3)=99.40(9),C(methyl)−Si−C(quinone)=108.20(10)−112.32(10).

the planes defined by C1−C2−C3′ and C2−C3−C2′−C3′ in **1d** was 18.0(3)°.

In contrast to the chair conformations of **1c** and **1d**, **3** assumed a rigid planar conformation due to the CH_2 bridge joining neighboring pairs of silicon atoms, as shown in Figure 3. The torsion angles of Si1−C2═C3′−Si2′ and C1−C2═C3′−C1′ were 0.6(2)° and 0.5(2)°, respectively. The angle between the planes defined by C1−C2−C3 and C2−C3−C2′−C3′ was 0.8(4)°. The narrower angles of C2−Si1−C4 [99.27(9)°] and C3−Si2−C4′ [99.40(9)°] indicate that the strain energy of the five-membered ring may induce structural effects on the molecule. Thus, the stretched C2═C3′ bond [1.362(3) Å] of **3** was attributed to the ring strain energy.

Figure 4 shows that **4** has an asymmetrically deformed structure. The C1−C2═C3−C4, C4−C5═C6−C1, and Si1−C2═C3−Si2 torsion angles were 21.3(7)°, 1.8(7)°, and 23.5(7)°, respectively. The angle between the planes defined by C1−C2−C6 and C2−C3−C5−C6 was 15.1(5)°. In contrast, the angle between the plane defined by C3−C4−C5 and C2−C3−C5−C6 was 6.8(5)°.

ORTEP drawings of 2,5-bis(trimethylgermyl)-1,4-benzoquinone (**5c**), 2,5-bis(dimethylvinylsilyl)-1,4-benzoquinone (**5d**), and 2,5-bis(dimethylphenylsilyl)-1,4-benzoquinone (**5e**) are shown in Figures 5−7, respectively. The asymmetric units of **5d** contain two types of crystallographically independent molecules. The two molecules have fundamentally similar structures, and therefore, only one of the two molecules (molecule A) is shown in Figure 6. Compounds **5c**−**e** had planar structures. The structural features of **5c**−**e** were similar to those of 2,5-bis(trimethylsilyl)-1,4-benzoquinone (**5a**),[3b] as summarized in Table 2.

Quinones **1c**, **1d**, and **4** were observed to be in the chair conformation, while **3** and **5c**−**e** were found to have planar structures. The origin of the difference between the chair conformation (for **1c**, **1d**, and **4**) and the planar geometry (**1b** and **5c**−**e**) should be explained by the steric repulsion between the vicinal substituents, because tetrakis(trimethylsilyl)ethylene,[12c] hexakis-(trimethylsilyl)benzene,[12d] and tetrakis(trimethylsilyl)-1,4-benzoquinone (**1a**)[8,9] have distorted structures due to the steric effects of trimethylsilyl groups. In the case of **3**, the rigidity of two five-membered rings should give rise to the planar structure. In summary the σ[$C_{quinone}$−

(11) (a) Sekiguchi, A.; Ebata, K.; Kabuto, C.; Sakurai, H. *J. Am. Chem. Soc.* **1991**, *113*, 1464. (b) Sakurai, H. *Pure Appl. Chem.* **1994**, *66*, 1431. (c) Setaka, W.; Ebata, K.; Sakurai, H.; Kira, M. *J. Am. Chem. Soc.* **2000**, *122*, 7781.

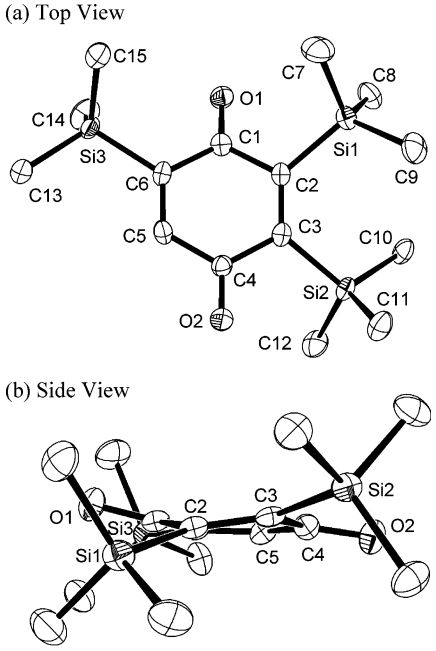

Figure 4. Top (a) and side (b) ORTEP views of **4** showing the atom-numbering scheme. Thermal ellipsoids are drawn at the 50% probability level. Hydrogen atoms are omitted for clarity. Selected bond lengths (Å): C(1)−O(1) = 1.214(6), C(1)−C(6) = 1.477(7), C(1)−C(2) = 1.497(7), C(2)−C(3) = 1.354(7), C(2)−Si(1) = 1.913(5), C(3)−C(4) = 1.498(7), C(3)−Si(2) = 1.904(5), C(4)−O(2) = 1.223(6), C(4)−C(5) = 1.479(7), C(5)−C(6) = 1.329(7), C(6)−Si(3) = 1.893(5), C(methyl)−Si(1) = 1.848(6)−1.869(6). Selected bond angles (deg): O(1)−C(1)−C(6) = 119.8(5), O(1)−C(1)−C(2) = 118.5(4), C(6)−C(1)−C(2) = 121.6(4), C(3)−C(2)−C(1) = 117.9(4), C(3)−C(2)−Si(1) = 130.4(4), C(1)−C(2)−Si(1) = 111.6(3), C(2)−C(3)−C(4) = 117.3(4), C(2)−C(3)−Si(2) = 130.8(4), C(4)−C(3)−Si(2) = 111.9(3), O(2)−C(4)−C(5) = 119.3(5), O(2)−C(4)−C(3) = 119.9(5), C(5)−C(4)−C(3) = 120.5(4), C(6)−C(5)−C(4) = 121.8(5), C(5)−C(6)−C(1) = 117.3(5), C(5)−C(6)−Si(3) = 124.7(4), C(1)−C(6)−Si(3) = 118.0(4), C(methyl)−Si−C(methyl) = 103.9(3)−112.4(3), C(methyl)−Si(1)−C(quinone) = 107.6(3)−111.4(2).

Si(or Ge)]−π* transition bands[8,9] observed in the UV−vis spectra of **1a**, **1c**, **1d**, and **4** were confirmed to be due to quinone ring deformations.

Cyclic Voltammetry. The half-wave reduction potentials ($E_{1/2}^{I}$ and $E_{1/2}^{II}$) of 1,4-benzoquinone derivatives were measured in an acetonitrile solution containing tetra-*n*-butylammonium perchlororate as the supporting electrolyte, referred to an Ag/Ag^+ (10 mM) redox couple. The $E_{1/2}$ values were determined using the equation $E_{1/2} = (E_{pa} + E_{pc})/2$, where E_{pa} and E_{pc} represent the anodic and cathodic peak potentials, respectively. Table 3 shows the data obtained from the cyclic voltammograms of 1,4-benzoquinone (**1f**), 2,5-bis(trimethylsilyl)-1,4-benzoquinone (**5a**), 2,5-di-*tert*-butyl-1,4-benzoquinone (**5g**), and 2-(trimethylsilyl)-1,4-benzoquinone (**6a**). As can be seen in the table, two sets of reversible redox peaks were present, which are thought to correspond to 1,4-benzoquinone/semiquinone ($E_{1/2}^{I}$) and semiquinone/hydroquinone dianion ($E_{1/2}^{II}$) couples. The first reduction step for 2,3,5,6-tetrakis(trimethylsilyl)quinone (**1a**) was reversible, while the second step was irreversible. This is thought to be due to chemical reactions that may occur

(12) (a) Sakurai, H.; Nakadaira, Y.; Kira, M.; Tobita, H. *Tetrahedron Lett.* **1980**, *21*, 3077. (b) Sakurai, H.; Tobita, H.; Kira, M.; Nakadaira, Y. *Angew. Chem., Int. Ed. Engl.* **1980**, *19*, 620. (c) Sakurai, H.; Nakadaira, Y.; Tobita, H.; Ito, T.; Toriumi, K.; Ito, H. *J. Am. Chem. Soc.* **1982**, *104*, 300. (d) Sakurai, H.; Ebata, K.; Kabuto, C.; Sekiguchi, A. *J. Am. Chem. Soc.* **1990**, *112*, 1799. (d) Sekiguchi, A.; Matsuo, T. *J. Synth. Org. Chem. Jpn.* **1999**, *57*, 53. (e) Sekiguchi, A.; Matsuo, T.; Watanabe, H. *J. Am. Chem. Soc.* **2000**, *122*, 565.

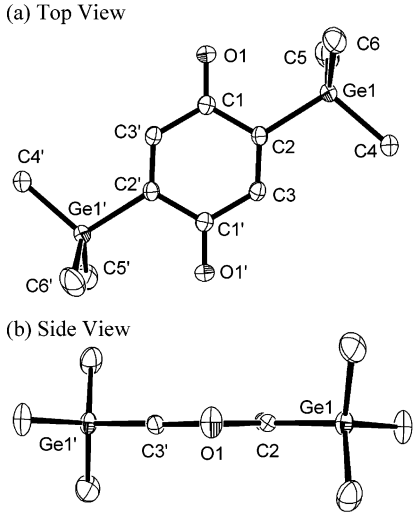

Figure 5. Top (a) and side (b) ORTEP views of **5c** showing the atom-numbering scheme. Dashes indicate atoms related by symmetry. Thermal ellipsoids are drawn at the 50% probability level. Hydrogen atoms are omitted for clarity. Selected bond lengths (Å): C(1)−O(1) = 1.225(3), C(1)−C(3)′ = 1.477(3), C(1)−C(2) = 1.480(3), C(2)−C(3) = 1.336(3), C(2)−Ge(1) = 1.961(2), C(methyl)−Ge(1) = 1.929(3)−1.935(3). Selected bond angles (deg): O(1)−C(1)−C(3)′ = 120.1(2), O(1)−C(1)−C(2) = 120.3(2), C(3)′−C(1)−C(2) = 119.62(19), C(3)−C(2)−C(1) = 117.9(2), C(3)−C(2)−Ge(1) = 124.25(16), C(1)−C(2)−Ge(1) = 117.89(16), C(2)−C(3)−C(1)′ = 122.5(2), C(methyl)−Ge(1)−C(methyl) = 110.22(12)−111.51(13), C(methyl)−Ge(1)−C(2) = 106.76(10)−108.79(11).

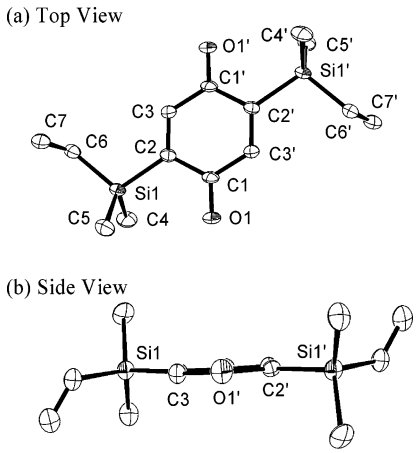

Figure 6. Top (a) and side (b) ORTEP views of **5d**, molecule A showing the atom-numbering scheme. Dashes indicate atoms related by symmetry. Thermal ellipsoids are drawn at the 50% probability level. Hydrogen atoms are omitted for clarity. Selected bond lengths (Å): C(1)−O(1) =1.233(4), C(1)−C(3)′ = 1.473(4), C(1)−C(2) = 1.483(4), C(2)−C(3) = 1.338(4), C(2)−Si(1) = 1.888(3), C(4)−Si(1) = 1.858(3), C(5)−Si(1) = 1.849(4), C(6)−C(7) = 1.319(5), C(6)−Si(1) = 1.849(3). Selected bond angles (deg): O(1)−C(1)−C(3)′= 119.5(3), O(1)−C(1)−C(2) = 120.2(3), C(3)′−C(1)−C(2) = 120.3(3), C(3)−C(2)−C(1) = 117.4(3), C(3)−C(2)−Si(1) = 123.7(3), C(1)−C(2)−Si(1) = 118.9(2), C(2)−C(3)−C(1)′ = 122.3(3), C(7)−C(6)−Si(1) = 123.7(3).

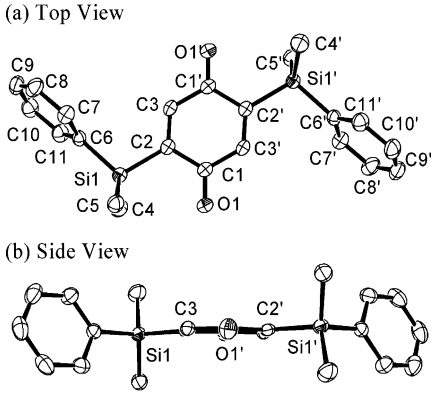

Figure 7. Top (a) and side (b) ORTEP views of **5e** showing the atom-numbering scheme. Dashes indicate atoms related by symmetry. Thermal ellipsoids are drawn at the 50% probability level. Hydrogen atoms are omitted for clarity. Selected bond lengths (Å): C(1)−O(1) =1.222(2), C(1)−C(3)′ = 1.482(3), C(1)−C(2) = 1.487(2), C(2)−C(3) = 1.334(3), C(2)−Si(1) = 1.893(2), C(4)−Si(1) = 1.852(2), C(5)−Si(1) = 1.859(2), C(6)−Si(1) = 1.867(2), C(phenyl)−C(phenyl) = 1.371(4)−1.399(3). Selected bond angles (deg): O(1)−C(1)−C(3)′= 120.25(16), O(1)−C(1)−C(2) = 120.87(17), C(3)′−C(1)−C(2) = 118.86(16), C(3)−C(2)−C(1) = 117.42(16), C(3)−C(2)−Si(1) = 124.39(14), C(1)−C(2)−Si(1) = 118.18(14), C(2)−C(3)−C(1)′ = 123.65(16), C(phenyl)−C(phenyl)−C(phenyl) = 117.03(18)−121.5(2).

Table 1. Selected Average Bond Lengths and Angles (Å and deg) for 1a−d and 3

	1a[b]	**1b**[b]	**1c**	**1d**	**3**
R−C[a]	1.911	1.894	1.983	1.911	1.905
C−C	1.501	1.498	1.502	1.497	1.495
C═C	1.354	1.351	1.365	1.360	1.362
C═O	1.225	1.215	1.216	1.227	1.235
R−C−C(O)[a]	112.2	112.6	112.3	113.1	123.5
R−C═C[a]	131.2	128.9	130.5	130.2	116.2
C(O)−C═C	116.6	118.5	117.2	116.7	120.4
C−C(O)−C	123.4	122.7	122.7	123.7	119.3
R−C═C−R[a]	17.3	2.8	14.0	22.1	0.6
C−C═C−C	20.0	3.7	18.8	18.8	0.5

[a] R = Si or Ge. [b] Reference 9.

Table 2. Selected Average Bond Lengths and Angles (Å and deg) for 5a and 5c−e

	5a[b]	**5c**	**5d**	**5e**
R−C[a]	1.873	1.961	1.884	1.893
C−C(R)[a]	1.487	1.480	1.483	1.487
C═C	1.347	1.336	1.342	1.334
C−C(H)	1.461	1.477	1.468	1.482
C═O	1.233	1.225	1.233	1.222
R−C−C(O)[a]	119.9	117.9	119.3	118.2
R−C═C[a]	124.5	124.3	123.6	124.4
C−C(R)═C[a]	115.6	117.9	117.1	117.4
C(R)═C−C[a]	123.7	122.5	122.6	123.7
C−C(O)−C	120.8	119.6	120.3	118.9
C−C═C−C	0.5	1.2	1.2	3.1

[a] R = Si or Ge. [b] Reference 3b.

after the second step. The $E_{1/2}^{I}$'s of **6a**, **5a**, and **1a** shifted negatively relative to **1f** by −0.04, −0.07, and −0.31 V, respectively. The $E_{1/2}^{II}$'s of **6a** and **5a** also shifted negatively relative to **1f** by −0.05 and −0.07 V, respectively. The $E_{1/2}^{I}$ and $E_{1/2}^{II}$ were observed to have an increasingly negative shift as the number of silyl substituents increased. The results indicate that the silyl group acted as an electron-donating group to the 1,4-benzoquinone and the semiquinone radical units.

Table 3. Peak Potentials of 1,4-Benzoquinones in Acetonitrile,[a] Referred to Ag/Ag$^+$

compd	E_{pc}^{I}	E_{pa}^{I}	$E_{1/2}^{I}$	E_{pa}^{II}	E_{pc}^{II}	$E_{1/2}^{II}$
1a	−1.17	−1.06	−1.12 [−0.83]	−1.76		irreversible
5a	−0.94	−0.82	−0.88 [−0.59]	−1.61	−1.48	−1.55 [−1.26]
6a	−0.91	−0.78	−0.85 [−0.56]	−1.62	−1.44	−1.53 [−1.24]
1f	−0.87	−0.75	−0.81 [−0.52]	−1.56	−1.40	−1.48 [−1.19]
5g	−1.07	−0.96	−1.02 [−0.73]	−1.81	−1.66	−1.74 [−1.45]

[a] 1,4-Benzoquinone derivatives: 3 mM; base solution: acetonitrile supplemented with 100 mM *n*-Bu_4NClO_4; WE: glassy carbon; RE: $Ag/AgNO_3$ (10 mM) redox couple in base solution; sweep rate: 100 mV/s. Values in brackets were calibrated to SCE (−0.29 V vs Ag/Ag$^+$).

Table 4. Bond Lengths and Angles (Å and deg) for 1h[opt] and 1h[exp] Optimized at the B3LYP/6-31G(d) Level

	1h[opt]	**1h[exp]**
Si−C	1.910	1.911
C−C	1.496	1.501
C═C	1.358	1.354
C═O	1.232	1.225
Si−C−C	111.1	112.2
Si−C═C	130.1	131.2
C−C═C	118.8	116.6
C−C(O)−C	122.5	123.4
Si−C═C−Si	0.0	17.3
C−C═C−C	0.0	20.0

The redox couple of **5a** and its corresponding semiquinone appears at a more positive potential than that of **5g** and its semiquinone, indicating that **5a** is a stronger electron-acceptor than **5g**. These findings are inexplicable when considering the inductive effect ($+I_{SiR3} > +I_{CR3}$) alone. As described below, additional $\sigma^*-\pi^*$ interactions[14] between the σ^*-orbital of the $Si-C_{quinone}$ bond and the lowest unoccupied or singly occupied molecular orbital of the 1,4-benzoquinone π-system may contribute to the lower reduction potentials observed in **5a** as compared to those of **5g**.

DFT Calculations for Silyl-Substituted Quinones. DFT calculations for 2,3,5,6-tetrakis(trihydrosilyl)-1,4-benzoquinone (**1h**) at the B3LYP/6-31G(d) level revealed that the optimized structure **1h[opt]** had a planar structure. The structural features for **1h[opt]**, summarized in Table 4, reproduced those of 2,3,5,6-tetrakis(dimethylsilyl)-1,4-benzoquinone (**1b**, Table 2). Quinone **1h[opt]** has D_{2h} symmetry, suggesting that the asymmetrical deformation from D_{2h} to C_1 in **1b** was due to the steric hindrance between the pairs of vicinal dimethylsilyl groups. To elucidate the energy and electronic structure of the chair conformation of 2,3,5,6-tetrakis(trimethylsilyl)-1,4-benzoquinone (**1a**), the molecular orbital calculations were carried out for **1h[exp]**, where the coordinates of the six carbon, two oxygen, and four silicon atoms in **1h** were fixed to those observed for **1a**, as summarized in Table 4. Because **1h[exp]** was

(13) (a) Bedford, J. A.; Bolton, J. R.; Carrington, A. C.; Prince, R. H. *Trans. Faraday Soc.* **1995**, *59*, 53. (b) Gerson, F.; Heinzer, J.; Bock, H.; Alt, H.; Seidl, H. *Helv. Chim. Acta* **1968**, *51*, 707. (c) Setaka, W.; Kabuto, C.; Kira, M. *Chem. Lett.* **1999**, 317. (d) Bock, H.; Ansari, M.; Nagel, N.; Havlas, Z. *J. Organomet. Chem.* **1995**, *499*, 63. (e) Setaka, W.; Kira, M. *Chem. Phys. Lett.* **2002**, *363*, 447.

(14) (a) Apeloig, Y. In *The Chemistry of Organic Silicon Compounds*; Patai, S., Rappoport, Z., Eds.; John Wiley: New York, 1989; Part 1, Chapter 2, and references therein. (b) Pitt, C. G. *J. Organomet. Chem.* **1973**, *61*, 49. (c) Pitt, C. G. *J. Organomet. Chem.* **1970**, *23*, C35. (d) Schleyer, P. v. R.; Clark, T.; Kos, A. J.; Spitznagel, G. W.; Rohde, C.; Arad, D.; Houk, K. N.; Rondan, N. G. *J. Am. Chem. Soc.* **1984**, *106*, 6467. (e) Setaka, W.; Kabuto, C.; Kira, M. *Chem. Lett.* **1999**, 317.

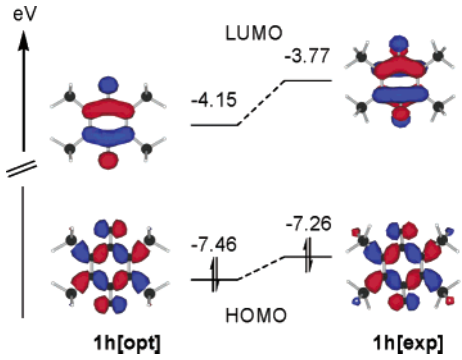

Figure 8. Schematic molecular orbitals and energy levels for **1h[opt]** and **1h[exp]** at the B3LYP/6-311++G(d,p)//B3LYP/6-31G(d) level.

Table 5. Bond Lengths and Angles (Å and deg) for 1a Optimized at the B3LYP/6-31G(d) Level

Si−$C_{quinone}$	1.931
C−C	1.500
C=C	1.364
C=O	1.234
Si−C−C	112.6
Si−C=C	131.0
C−C=C	116.5
C−C(O)−C	123.8
Si−C=C−Si	16.9
C−C=C−C	19.5

only 4.8 kcal mol^{-1} higher in energy than **1h[opt]** at the B3LYP/6-311++G(d,p)//B3LYP/6-31G(d) level, the conformational change from a planar structure to a chair conformation will be feasible by the steric effects.

The energy levels of the highest occupied molecular orbitals (HOMOs) and the lowest unoccupied molecular orbitals (LUMOs) for **1h[opt]** and **1h[exp]** are schematically shown in Figure 8. The shapes of HOMO and LUMO for **1h[exp]** were similar to those for **1h[opt]**, but **1h[exp]** had a higher-lying HOMO (by 0.20 eV) and a much higher-lying LUMO (by 0.38 eV). The deformation of the quinone ring in **1h[exp]** would cause the energy differences between **1h[opt]** and **1h[exp]**.

Next, the structures of 2,3,5,6-tetrakis(trimethylsilyl)-1,4-benzoquinonoe (**1a**), 2,5-bis(trimethylsilyl)-1,4-benzoquinonoe (**5a**), 2-(trimethylsilyl)-1,4-benzoquinone (**6a**), 1,4-benzoquinone (**1f**), and 2,5-di-*tert*-butyl-1,4-benzoquinone (**5g**) were computed at the B3LYP/6-31G(d) level. The optimized structures of **5a**, **6a**, **1f**, and **5g** had planar structures, while that of **1a** took the chair conformation. As listed in Table 5, the structural features for the solid-state structure of **1a** were fundamentally reproduced by the optimized **1a** with C_{2h} symmetry.

The vibrational frequencies of the carbonyl units and the HOMO and LUMO energy levels of **1a**, **5a**, **6a**, **1f**, and **5g** are summarized in Table 6. The shapes of the HOMO and LUMO for **1a** were essentially similar to those for **1h[exp]**. IR absorption frequencies of the C=O units in **1a** (1618 cm^{-1}),[9] **5a** (1643 cm^{-1}),[9] **6a** (1662 and 1651 cm^{-1}), **1f** (1668 and 1656 cm^{-1}),[15] and **5g** (1656 cm^{-1})[16] were in good agreement with the computed vibrational frequencies. The LUMO energy levels of **1a**, **5a**, **6a**, **1f**, and **5g** were estimated to be −3.27, −3.68, −3.82, −3.99, and −3.58 eV, respectively. The order of the $E_{1/2}^{I}$'s for **1a**, **5g**, **5a**, **6a**, and **1f** was consistent with the order expected for the corresponding LUMO energy levels. The HOMOs and the LUMOs shifted to higher energies as the number of silyl groups increased, whereas the calculated vibrational frequencies shifted to lower frequencies. The result of calculations indicates that the silyl groups acted as electron-donating substituents.

Table 6. Summary of Energetics of the 1,4-Benzoquinone Systems Calculated at the B3LYP/6-311++G(d,p)//B3LYP/6-31G(d) Level

	1a	5a	6a	1f	5g
LUMO/eV	−3.26	−3.68	−3.82	−3.99	−3.58
HOMO/eV	−6.47	−7.18	−7.48	−7.83	−7.33
vibrational frequency/cm^{-1}	1625	1660	1684, 1664	1690	1665
IR $\nu_{C=O}$/cm^{-1}	1618[a]	1643[a]	1662, 1651	1668, 1656[b]	1656[c]

[a] Reference 9. [b] Reference 15. [c] Reference 16.

Trialkylsilyl substituents are known to electronically stabilize aromatic π anions[11,12] and anion radicals.[13] This is demonstrated by the readily obtained hexasilylbenzene dianion complexes upon lithium reduction of the corresponding hexasilylbenzene.[11] DFT calculations also gave the LUMO energy of trimethylsilylbenzene (−0.68 eV) lower than that of benzene (−0.49 eV). The result is explained by the $\pi^*-\sigma^*$(Si−C) conjugation in the former.[14] However, in the silylquinone system, trimethylsilyl groups raised the LUMO energy level. The increase in the energy of the LUMO of the trimethylsilyl-substituted quinone can be explained by the inductive effect of the silyl group. The π^* energy level of quinone (**1f**, −3.99 eV) was much lower than that of benzene (−0.49 eV). Therefore, the degree of $\pi^*-\sigma^*$(Si−C) conjugation should be small in this system. The sum of the inductive effect and the $\pi^*-\sigma^*$ interaction in the silyl group is responsible for the higher LUMO energy level of silylquinone. Because the energy level of the σ^*-(C−C) orbital is higher than that of the σ^*(Si−C) orbital, the $\pi^*-\sigma^*$(C−C) conjugation in **5g** is less effective than the $\pi^*-\sigma^*$(Si−C) conjugation in **5a**. As a result, the LUMO energy level of **5g**, having *tert*-butyl groups, which are less positive than trimethylsilyl groups, was estimated to be 0.1 eV lower than that of **5a** (Table 6). As descried above, DFT calculations for **1h[opt]** and **1h[exp]** demonstrated that the deformation of the quinone ring destabilizes the LUMO energy level. In **1a**, the deformation of the quinone ring and the introduction of four trimethylsilyl groups were responsible for the higher LUMO energy level.

Conclusion

By X-ray crystallographic analysis, it was proved that 2,3,5,6-tetrakis(trimethylgermyl)-1,4-benzoquinone (**1c**), 2,3,5,6-tetrakis(dimethylvinylsilyl)-1,4-benzoquinone (**1d**), and 2,3,5-tris(trimethylsilyl)-1,4-benzoquinone (**4**) were in a more stable chair conformation. In contrast to these compounds, 4,4,6,6,10,10,12,12-octamethyl-4,6,10,12-tetrasilatricyclo[7.3.0.$0^{3,7}$]dodeca-1(9),3(7)-diene-2,8-dione (**3**), 2,5-bis(trimethylgermyl)-1,4-benzoquinone (**5c**), 2,5-bis(dimethylvinylsilyl)-1,4-benzoquinone (**5d**), and 2,5-bis(dimethylphenylsilyl)-1,4-benzoquinone (**5e**) had planar structures. The $\sigma-\pi^*$ transition bands observed in the UV−vis spectra of **1a**, **1c**, **1d**, and **4** were thought to be a result of deformed structures. Cyclic voltammograms of 1,4-benzoquinone (**1f**) and 2,5-bis(trimethyl-

(15) Charney, E.; Becker, E. D. *J. Chem. Phys.* **1965**, *42*, 910.

silyl)-1,4-benzoquinone (**5a**) showed two sets of reversible redox peaks. On the other hand, the voltammogram of 2,3,5,6-tetrakis(trimethylsilyl)-1,4-benzoquinone (**1a**) showed that the first reduction step was reversible and the second reduction step was irreversible. The first reduction potential in **1a** ($E_{1/2}^{I} = -1.12$ V vs Ag/Ag^+) was higher by more than 0.2 V compared to those of **5a** ($E_{1/2}^{I} = -0.88$ V) and **1f** ($E_{1/2}^{I} = -0.81$ V). DFT calculations for trimethylsilyl-substituted 1,4-benzoquinones indicated that the LUMOs shifted to higher energies, whereas the calculated vibrational frequencies shifted to lower frequencies as the number of silyl groups increased. These results indicate that the trimethylsilyl group acted as an electron-donating group to the 1,4-benzoquinone unit. DFT calculations for **1h-[opt]** and **1h[exp]** demonstrated that the deformation of the ring in **1a**, due to the steric repulsion of pairs of vicinal trimethylsilyl groups, resulted in an increase in the HOMO energy level.

Further investigations on the properties of silyl- and germyl-1,4-benzoquinones are currently underway.

Experimental Section

General Methods. ^{1}H, ^{13}C, and ^{29}Si NMR spectra were recorded on a Varian INOVA 300 FT-NMR spectrometer at 300, 75.4, and 59.6 MHz, respectively. Mass spectra were recorded on Shimadzu GCMS-QP5050A and HITACHI M-2500 mass spectrometers. IR spectra were recorded on a JEOL JIR-3505/3510 system. Gel permeation chromatography (GPC) was conducted on a LC908-C60 recycling high-pressure liquid chromatograph (Japan Analytical Instruments, Co. Ltd.) using JAIGEL-1H (40 mm × 600 mm), JAIGEL-2H (40 mm × 600 mm), and JAIGEL-2.5H (40 mm × 600 mm) columns, using chloroform as an eluent.

Materials. 2,3,5,6-Tetrakis(trimethylgermyl)-1,4-benzoquinone (**1c**), 2,3,5,6-tetrakis(dimethylvinylsilyl)-1,4-benzoquinone (**1d**), 4,4,6,6,10,10,12,12-octamethyl-4,6,10,12-tetrasilatricyclo[7.3.0.0^{3,7}]dodeca-1(9),3(7)-diene-2,8-dione (**3**), 2,3,5-tris(trimethylsilyl)-1,4-benzoquinone (**4**), 2,5-bis(trimethylgermyl)-1,4-benzoquinone (**5c**), 2,5-bis(dimethylvinylsilyl)-1,4-benzoquinone (**5d**), and 2,5-bis(dimethylphenylsilyl)-1,4-benzoquinone (**5e**) were prepared according to the procedures previously reported.[9] TMEDA, CH_3CN, CH_2Cl_2, $CHCl_3$, MeOH, $CDCl_3$, Me_2SiCl_2, 2,5-di-*tert*-butyl-1,4-benzoquinone, 1,4-dimethoxybenzene, tetra-*n*-butylammonium perchlorate, *n*-BuLi (in hexane), anhydrous magnesium sulfate, cerium ammonium nitrate (CAN), $NaHCO_3$, THF, and Et_2O were commercially available.

Preparation of 1,4-Dimethoxy-2-(trimethylsilyl)benzene. A hexane solution of *n*-BuLi (55.6 mL, 83.4 mmol) was added to a mixture of 1,4-dimethoxybenzene (11.0 g, 79.6 mmol), TMEDA (14 mL, 92.8 mmol), and Et_2O (350 mL) at room temperature. After stirring for 15 h, a mixture of Me_3SiCl (10.3 g, 95.2 mmol) and Et_2O (20 mL) was added to the mixture. The mixture was stirred for 4 h and subsequently hydrolyzed with water. The organic layer was separated, and the aqueous layer was extracted with hexane (200 mL). The organic layer and the extracts were combined, washed with water and brine, dried over anhydrous magnesium sulfate, and filtered. The filtrate was concentrated under reduced pressure. Distillation yielded 1,4-dimethoxy-2-(trimethylsilyl)benzene (15.1 g, 71.5 mmol, 90%):[17] colorless oil; bp 70−100 °C/1 mmHg; ^{1}H NMR ($CDCl_3$, δ) 0.26 (s, 9H), 3.76 (s, 3H), 3.77 (s, 3H), 6.76 (d, J = 12 Hz, 1H), 6.50 (dd, J = 12 and 4 Hz, 1H), 6.95 (d, J = 4 Hz, 1H); ^{13}C NMR ($CDCl_3$, δ) −1.05, 55.65, 55.70, 110.40, 114.84, 121.13, 129.42, 153.37, 158.55; ^{29}Si NMR ($CDCl_3$, δ) −4.73; MS (70 eV) *m*/*z* 210 (M^+).

Preparation of 2-(Trimethylsilyl)-1,4-benzoquinone (6a). A mixture of 1,4-dimethoxy-2-(trimethylsilyl)benzene (680 mg, 3.23 mmol), CAN (5.86 g, 10.7 mmol), CH_3CN (150 mL), and H_2O (150 mL) was stirred at room temperature for 16 h. The mixture was hydrolyzed with water. The organic layer was separated, and the aqueous layer was extracted with $CHCl_3$ (150 mL). The organic layer and the extracts were combined, washed with aqueous $NaHCO_3$, water, and brine, dried over anhydrous magnesium sulfate, and filtered. The filtrate was concentrated under reduced pressure and separated by using a recycling GPC ($CHCl_3$ as an eluent) to give **6a**[2] (351 mg, 1.94 mmol, 60%): orange crystals; ^{1}H NMR ($CDCl_3$, δ) 0.23 (s, 9H), 6.7−6.75 (m, 2H), 6.86 (d, J = 2 Hz, 1H); ^{13}C NMR ($CDCl_3$, δ) −1.80, 136.28, 137.97, 143.29, 152.43, 186.70, 190.83; ^{29}Si NMR ($CDCl_3$, δ) −3.27; MS (70 eV) *m*/*z* 180 (M^+).

Preparation of 1,4-Dimethoxy-2,5-bis(trimethylsilyl)-benzene. A hexane solution of *n*-BuLi (43.0 mL, 64.5 mmol) was added to a mixture of 1,4-dimethoxybenzene (4.03 g, 29.2 mmol), TMEDA (10 mL, 66.3 mmol), and Et_2O (200 mL) at room temperature. After it was stirred for 18 h, a mixture of Me_3SiCl (7.64 g, 70.3 mmol) and Et_2O (10 mL) was added to the mixture. The mixture was stirred for 5 h and subsequently hydrolyzed with water. The organic layer was separated, and the aqueous layer was extracted with hexane (100 mL). The organic layer and the extracts were combined, washed with aqueous $NaHCO_3$, water, and brine, dried over anhydrous magnesium sulfate, and filtered. The filtrate was concentrated under reduced pressure. Recrystallization with MeOH yielded 1,4-dimethyoxy-2,5-bis(trimethylsilyl)benzene (4.34 g, 15.4 mmol, 53%):[17] colorless crystals; ^{1}H NMR ($CDCl_3$, δ) 0.25 (s, 18H), 3.77 (s, 6H), 6.84 (s, 2H); ^{13}C NMR ($CDCl_3$, δ) −1.00, 55.83, 116.25, 130.20, 158.34; ^{29}Si NMR ($CDCl_3$, δ) −4.88; MS (70 eV) *m*/*z* 282 (M^+).

Preparation of 2,5-Bis(trimethylsilyl)-1,4-benzoquinone (5a). A mixture of 2,5-bis(trimethylsilyl)-1,4-dimethoxybenzene (212 mg, 0.750 mmol), CAN (1.14 g, 2.08 mmol), CH_3CN (25 mL), and H_2O (15 mL) was stirred at room temperature for 2.5 h. The mixture was hydrolyzed with water. The organic layer was separated, and the aqueous layer was extracted with $CHCl_3$ (50 mL). The organic layer and the extracts were combined, washed with water and brine, dried over anhydrous magnesium sulfate, and filtered. The filtrate was concentrated under reduced pressure, and the residue was purified using silica gel chromatography with a mixture of toluene/hexane as the eluent to yield **5a** (171 mg, 0.678 mmol, 90%):[3] orange crystals; ^{1}H NMR ($CDCl_3$, δ) 0.22 (s, 18H), 6.84 (s, 2H); ^{13}C NMR ($CDCl_3$, δ) −1.81, 144.79, 151.76, 190.13; ^{29}Si NMR ($CDCl_3$, δ) −3.81; MS (70 eV) m/z 252 (M^+).

X-ray Structure Determinations of Silyl- and Germyl-1,4-benzoquinones. Single crystals of **1c**, **1d**, **3**, **4**, and **5c**−**e**, suitable for X-ray crystallographic analysis, were obtained from the hexane solutions. Intensity data were collected on a Bruker SMART 1000 CCD system[18] using graphite-monochromatized Mo Kα radiation (λ = 0.71073 Å). Data integration was accomplished using the SAINT program.[19] The empirical method was employed for absorption correction using the SADABS program.[20] Subsequent calculations were carried out using the SHELXTL system.[21]

Crystal data for **1c**: $C_{18}H_{36}Ge_4O_2$, M = 574.83, deep red plates, 0.35 × 0.30 × 0.30 mm^3, Mo Kα (λ = 0.71073 Å),

(16) Rieker, A.; Rundel, W.; Kessler, H. *Z. Naturforsch.* **1969**, *24b*, 547.

(17) Crowther, G. P.; Sundberg, R. J.; Sarpeshkar, A. M. *J. Org. Chem.* **1984**, *49*, 4657.

(18) *SMART for Windows NT v5.054 Data Collection* and *SAINT+ for NT v5.00 Data Processing Software for the SMART system*; Bruker Analytical X-ray Instruments, Inc.: Madison, WI, 1998.

(19) *SAINT Software Reference Manual*, Version 4; Bruker Analytical X-ray Instruments, Inc.: Madison, WI, 1998.

(20) Sheldrick, G. M. *SADABS*; Bruker Analytical X-ray Instruments, Inc.: Madison, WI, 1998.

orthorhombic, space group = *Pbca*, a = 10.600(2) Å, b = 12.176(3) Å, c = 18.977(4) Å, V = 2449.2(9) Å^3, Z = 4, T = 123 K, D_{calc} = 1.559 g/cm^3, GOF = 0.907, R = 0.0531 [$I > 2\sigma(I)$], R = 0.1270 (all data).

Crystal data for **1d**: $C_{22}H_{36}O_2Si_4$; M = 444.87, deep red plates, 0.35 × 0.30 × 0.17 mm^3, Mo Kα (λ = 0.71073 Å), monoclinic, *P*2(1)/*c*, a = 11.7301(15) Å, b = 10.2316(13) Å, c = 11.8851(15) Å, β = 114.890(2)°, V = 1293.9(3) Å^3, Z = 2, D_{calc} = 1.142 g/cm^3, T = 123 K, GOF = 1.119, R = 0.0398 [$I > 2\sigma(I)$], R = 0.1224 (all data).

Crystal data for **3**: $C_{16}H_{28}O_2Si_4$; M = 364.74, purple plates; 0.35 × 0.20 × 0.15 mm^3, Mo Kα (λ = 0.71073 Å), orthorhombic; *Pbca*, a = 9.2970(19) Å, b = 11.214(2) Å, c = 19.780(4) Å, V = 2062.2(7) Å^3, Z = 4, D_{calc} = 1.175 g/cm^3, T = 123 K, GOF = 0.975, R = 0.0408 [$I > 2\sigma(I)$], R = 0.1066 (all data).

Crystal data for **4**: $C_{15}H_{28}O_2Si_3$, M = 324.64, deep red plate, 0.35 × 0.25 × 0.20 mm^3, orthorhombic, Mo Kα (λ = 0.71073 Å), space group = *Pbca*, a = 10.628(2) Å, b = 11.837(2) Å, c = 30.335(6) Å, V = 3816.1(12) Å^3, Z = 8, T = 123 K, D_c = 1.130 g/cm^3, GOF = 1.194, R = 0.0887 [$I > 2\sigma(I)$], R = 0.2263 (all data).

Crystal data for **5c**: $C_{12}H_{20}Ge_2O_2$, M = 341.46, orange needles, 0.30 × 0.30 × 0.20 mm^3, Mo Ka (λ = 0.71073 Å), monoclinic, space group = *P*2(1)/*n*, a = 6.7361(13) Å, b = 10.819(2) Å, c = 10.402(2) Å, β = 95.162(4)°, V = 755.0(3) Å^3, Z = 2, T = 123 K, D_c = 1.502 g/cm^3, GOF = 0.947, R = 0.0210 [$I > 2\sigma(I)$], R = 0.0507 (all data).

Crystal data for **5d**: $C_{14}H_{20}O_2Si_2$, M = 276.48, orange needles, 0.27 × 0.20 × 0.20 mm^3, Mo Kα (λ = 0.71073 Å), monoclinic, space group = *P*2(1)/*c*, a = 12.222(2) Å, b = 10.729(2) Å, c = 12.906(3) Å, β = 113.84(3)°, V = 1547.9(5) Å^3, Z = 4, T = 123 K, D_{calc} = 1.186 g/cm^3, GOF = 0.948, R = 0.0666 [$I > 2\sigma(I)$], R = 0.1681 (all data).

Crystal data for **5e**: $C_{22}H_{24}O_2Si_2$, M = 376.59, orange needles, 0.25 × 0.23 × 0.23 mm^3, Mo Kα (λ = 0.71073 Å), monoclinic, space group = *P*2(1)/*c*, a = 7.2992(14) Å, b = 6.4686(12) Å, c = 22.142(4) Å, β = 99.310(4)°, V = 1031.7(3) Å^3, Z = 2, T = 123 K, D_{calc} = 1.212 g/cm^3, GOF = 0.989, R = 0.0419 [$I > 2\sigma(I)$], R = 0.1070 (all data).

Cyclic Voltammetric Measurements. Voltammetric measurements were conducted with 3 mM 1,4-benzoquinones in a base solution under a nitrogen atmosphere. The base solution was acetonitrile containing 100 mM tetra-*n*-butylammonium perchlorate as the supporting electrolyte. The peak potentials listed in Table 3 were determined at a sweep rate of 100 mV/s using an Ag/AgNO$_3$ (10 mM) reference electrode. A glassy carbon disk (diameter; 5 mm) with a Teflon cap was used as the working electrode, and the surface of the disk was polished using alumina powders and washed with acetonitrile prior to each measurement. The $E_{1/2}$ values were determined as (E_{pa} + E_{pc})/2, where E_{pa} and E_{pc} represent the anodic and cathodic peak potentials, respectively.

Theoretical Calculations. All geometry optimizations and subsequent vibrational frequency calculations were performed at the B3LYP/6-31G(d) level. These were followed by single-point calculations at the B3LYP/6-311++G(d,p) level. The B3LYP calculations were performed using the Gaussian 03 program.[22] According to previous computational experience, vibrational frequencies computed at the B3LYP/6-31G(d) level were about 1−4% too high due to the harmonic oscillator approximation and the incomplete treatment of electron correlation effects.[23] Thus, the computed frequencies were multiplied by a correction factor of 0.9614 in order to correct for the anharmonicity of the vibrations.

Acknowledgment. A part of this work was supported by the Special Postdoctoral Researchers Program of RIKEN. We thank Dr. Eunsang Kwon and Dr. Hiromasa Tanaka (RIKEN) for fruitful discussions on the theoretical calculations.

Supporting Information Available: Tables are available listing the details of the X-ray structure determination, thermal ellipsoid plots, fractional atomic coordinates, anisotropic thermal parameters, bond lengths, and bond angles for **1c**, **1d**, **3**, **4**, and **5c**−**e**. This material is available free of charge via the Internet at http://pubs.acs.org.

OM034325A

(21) Sheldrick, G. M. *SHELXTL*; Bruker Analytical X-ray Instruments, Inc.: Madison, WI, 1997.

(22) Frisch, M. J.; Trucks, G. W.; Schlegel, H. B.; Scuseria, G. E.; Robb, M. A.; Cheeseman, J. R.; Montgomery, J. A., Jr.; Vreven, T.; Kudin, K. N.; Burant, J. C.; Millam, J. M.; Iyengar, S. S.; Tomasi, J.; Barone, V.; Mennucci, B.; Cossi, M.; Scalmani, G.; Rega, N.; Petersson, G. A.; Nakatsuji, H.; Hada, M.; Ehara, M.; Toyota, K.; Fukuda, R.; Hasegawa, J.; Ishida, M.; Nakajima, T.; Honda, Y.; Kitao, O.; Nakai, H.; Klene, M.; Li, X.; Knox, J. E.; Hratchian, H. P.; Cross, J. B.; Adamo, C.; Jaramillo, J.; Gomperts, R.; Stratmann, R. E.; Yazyev, O.; Austin, A. J.; Cammi, R.; Pomelli, C.; Ochterski, J. W.; Ayala, P. Y.; Morokuma, K.; Voth, G. A.; Salvador, P.; Dannenberg, J. J.; Zakrzewski, V. G.; Dapprich, S.; Daniels, A. D.; Strain, M. C.; Farkas, O.; Malick, D. K.; Rabuck, A. D.; Raghavachari, K.; Foresman, J. B.; Ortiz, J. V.; Cui, Q.; Baboul, A. G.; Clifford, S.; Cioslowski, J.; Stefanov, B. B.; Liu, G.; Liashenko, A.; Piskorz, P.; Komaromi, I.; Martin, R. L.; Fox, D. J.; Keith, T.; Al-Laham, M. A.; Peng, C. Y.; Nanayakkara, A.; Challacombe, M.; Gill, P. M. W.; Johnson, B.; Chen, W.; Wong, M. W.; Gonzalez, C.; Pople, J. A. *Gaussian 03*, revision B.03; Gaussian, Inc.: Pittsburgh, PA, 2003.

(23) Scott, A. P.; Radom, L. *J. Phys. Chem.* **1996**, *100*, 16502.